ELSEVIER

Journal of Alloys and Compounds 456 (2008) 57–63

Journal of ALLOYS AND COMPOUNDS

www.elsevier.com/locate/jallcom

Structural analysis and vacuum ultraviolet excited luminescence properties of sol–gel derived $Y_3Al_5O_{12}:Eu^{3+}$ phosphors

Chung-Hsin Lu [a,*], Wei-Tse Hsu [a], Chia-Hao Hsu [a], Hsiao-Chi Lu [b], Bing-Ming Cheng [b]

[a] *Electronic and Electro-optical Ceramics Laboratory, Department of Chemical Engineering, National Taiwan University, Taipei, Taiwan, ROC*
[b] *National Synchrotron Radiation Research Center, Hsinchu, Taiwan, ROC*

Received 20 October 2006; received in revised form 3 February 2007; accepted 5 February 2007
Available online 12 February 2007

Abstract

The structural and luminescence characteristics of sol–gel derived $Y_3Al_5O_{12}:Eu^{3+}$ ($YAG:Eu^{3+}$) phosphors were investigated using synchrotron radiation. VUV-excited luminescence studies reveal that two major excitation peaks formed at 178 and 238 nm are responsible for producing the characteristic red emission of Eu^{3+} ions. The emission characteristics of the sol–gel derived $YAG:Eu^{3+}$ phosphors depend significantly on the calcination temperature and cationic ratios. The Rietveld refinement analysis and luminescence studies indicate that increasing either the calcination temperature or the aluminum ion content can result in a more symmetrical anionic environment for Eu^{3+} ions in the YAG host, thereby enhancing the luminescence of the synthesized phosphors. $YAG:Eu^{3+}$ phosphors with reduced particle sizes and improved emission characteristics were successfully prepared in this study via controlling the calcination temperature and cationic ratios.

Keywords: Yttrium aluminum garnet; Phosphors; Sol–gel; Luminescence

1. Introduction

The development of new-generation, high-resolution displays demands phosphors with controlled morphology and enhanced luminescence properties. Yttrium aluminum garnet doped with europium ions ($Y_3Al_5O_{12}:Eu^{3+}$, $YAG:Eu^{3+}$) is an important phosphor because of its versatile applications in many luminescent and optical devices. The synthesis and luminescence properties of this phosphor prepared via the conventional solid-state route have been reported [1,2]. The results indicate that Eu^{3+} ions substitute at Y^{3+} sites in the YAG host and produce an intense red emission. The YAG-based phosphors prepared via the solid-state reaction are known to produce low luminescence due to the presence of impurity phases [3]. The as-prepared phosphors usually exhibit irregular morphology, large particle size, and wide particle size distribution. For application to new optical devices such as field emission displays (FED) and plasma display panels (PDP), phosphors need to have high emission intensity and small particle size with uniform narrow distribution [4].

Ultrafine $YAG:Eu^{3+}$ phosphors can be synthesized at low temperatures without coexistence of impurity phases using various soft chemical processes such as the sol–gel methods and the combustion method [5–10]. In most of the previous studies, UV-light was utilized to analyze the luminescence properties of the phosphors prepared via the soft chemical processes. The luminescence properties are highly dependent on the excitation wavelength. To be applicable to PDP devices, the phosphors must first be investigated under vacuum ultraviolet (VUV) excitation. Earlier studies on VUV excited luminescence have identified a 178 nm excitation band resulting from the intrinsic fundamental absorption of the YAG host for phosphors prepared via the conventional route [11]. However, VUV excited emission for the sol–gel derived phosphors and the effects of the preparation conditions have not been explored in detail.

In this study, $YAG:Eu^{3+}$ phosphors were prepared via a sol–gel process employing citric acid and ethylene glycol as the polymerizing agents. The prepared phosphors were investigated under VUV excitation to understand their luminescence properties. The effects of the calcination temperature and chemical compositions on the VUV excited luminescence of the prepared phosphors were also studied. The Rietveld refinement method [12] was employed to analyze the crystal structure. The sites

* Corresponding author.
E-mail address: chlu@ntu.edu.tw (C.-H. Lu).

0925-8388/$ – see front matter © 2007 Elsevier B.V. All rights reserved.
doi:10.1016/j.jallcom.2007.02.029

occupied by Eu^{3+} and defects in the prepared phosphors were determined according to the XRD data collected using high-intensity monochromatic synchrotron radiation.

2. Experimental

Yttrium aluminum garnet phosphors were prepared via the sol–gel process employing citric acid and ethylene glycol as the polymerizing agents. Analytical-grade yttrium nitrate and aluminum nitrate were individually dissolved in deionized water. Europium oxide was dissolved in dilute nitric acid. The concentrations of aluminum, yttrium and europium ions in the solutions were fixed at 0.25, 0.15 and 0.15 M, respectively. The prepared solutions were mixed in accordance with the ratio of Y^{3+}:Al^{3+}:Eu^{3+} = 2.85:*m*:0.15. The *m* value equals 4.5, 5.0 and 5.5 in systems I, II and III, respectively. When *m* equals 5, the prepared powders have a chemical formula of $(Y_{2.85}Eu_{0.15})Al_5O_{12}$. 0.5 M citric acid solution was used to chelate the metal ions and to polymerize with ethylene glycol to form gels. The metal nitrate and citric acid solutions were mixed and stirred for 1.5 h, followed adding ethylene glycol and citric acid into the solution. The mixed solution was then heated and stirred continuously on a hot plate at 130 °C for 1.5 h. This solution was then heated at 350 °C to evaporate excess water and initiate the polymerization reaction. A large amount of brownish gas was spurted, and the clear solution turned into white-yellowish gels. The precursors were obtained via grinding the dried gels.

The precursors were calcined at 800–1400 °C for 2 h. The phase purity and crystallinity of the obtained powders were analyzed using an X-ray diffractometer (XRD, MAC science MXP3). The morphology and particle sizes were examined using a scanning electron microscope (SEM, Hitachi S-800), respectively. High energy X-ray with λ = 1.32679 Å from synchrotron radiation was employed at National Synchrotron Radiation Research Center (NSRRC, Taiwan) to investigate the crystal structure of the non-stoichiometric YAG:Eu^{3+} phosphors. The VUV light produced in the center was dispersed with a high-flux cylindrical grating monochromator. The intensity of this VUV light was monitored by means of light reflected from a LiF beam splitter. A small fraction of the reflected beam passed one additional LiF plate and became incident on a glass window coated with sodium salicylate. The fluorescence signal was subsequently detected by a photomultiplier tube in a photon-counting mode.

3. Results and discussion

3.1. Structural and luminescence characteristics of YAG:Eu^{3+} phosphors

Fig. 1 illustrates the X-ray diffraction patterns of $(Y_{2.85}Eu_{0.15})Al_5O_{12}$ (in system II) calcined at various temperatures ranging from 800 to 1400 °C for 2 h. The XRD pattern for 800 °C-derived powder reveals amorphous structure (curve a). Fig. 1(b) reveals the presence of a cubic garnet phase for the powder calcined at 900 °C. The obtained diffraction pattern is consistent with the data reported for $Y_3Al_5O_{12}$ in the ICDD file No. 33-0040, indicating that single-phased YAG was successfully prepared with 900 °C-calcination. This temperature is 700 °C lower than that required in the conventional solid-state route [13]. No other intermediate phases are formed during the calcination processes, suggesting that the sol–gel derived precursors transform directly into the crystalline YAG phase without going through the complicated reaction processes reported in solid-state methods [14]. Due to thorough mixing of the starting materials in the sol–gel process, the required temperature for synthesizing YAG is markedly lowered and the reaction sequence is simplified. As shown in Fig. 1(b)–(e), the diffraction intensity of YAG:Eu^{3+} phosphor increases with raising the calcination temperature, revealing the enhancement in the crystallinity of the prepared samples. The crystallite sizes of the obtained phosphors were calculated using Scherrer's equation [15]. As illustrated in the inset of Fig. 1, the crystallite size is found to increase with raising the calcination temperature.

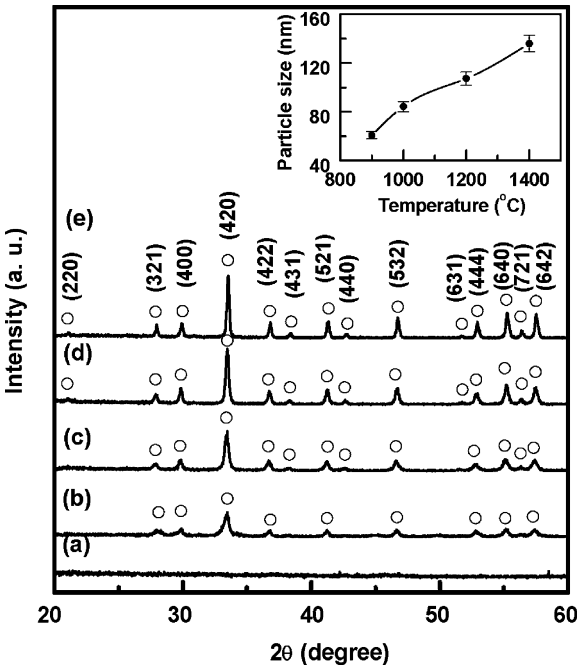

Fig. 1. X-ray diffraction patterns of the sol–gel derived $(Y_{2.85}Eu_{0.15})Al_5O_{12}$ phosphors calcined for 2 h at (a) 800 °C, (b) 900 °C, (c) 1000 °C, (d) 1200 °C, and (e) 1400 °C. Inset shows the dependence of the crystallite size on the calcination temperature.

The scanning electron micrographs of the prepared $(Y_{2.85}Eu_{0.15})Al_5O_{12}$ phosphors (system II) are shown in Fig. 2. Well-dispersed nanoparticles with a size around 60 nm were obtained after 900 °C-calcination for 2 h (Fig. 2(a)). As the calcination temperature increased to 1000 (Fig. 2(b)), 1200 (Fig. 2(c)) and 1400 °C (Fig. 2(d)), the particle sizes increased to around 90, 120 and 200 nm, respectively. Both of the particle size and crystallite size of YAG:Eu^{3+} phosphor increase with a rise in calcination temperatures. In the sol–gel process incorporating ethylene glycol as a polymerizing agent, numerous tiny cages are formed due to cross-linking reaction during polymerization. Cationic sols are trapped inside these tiny cages and subsequently convert into YAG crystallites during calcination, rendering restricted particle growth within the tiny cages. Therefore, the sol–gel route using polymerizing agent leads to the formation of nanosized particles.

Fig. 3 illustrates the emission spectra of the sol–gel derived YAG:Eu^{3+} (5%) phosphors (system II) calcined at temperature ranging from 900 to 1400 °C upon 147 nm VUV light excitation. The intensities of emissions were carefully normalized with the beam current of synchrotron. All the samples were studied under the same size and geometrical position. By this means, we can quantitatively compare the normalized intensities of the PL spectra for different samples. Similar emission spectra were observed for all samples. It was found that the emission intensities of YAG:Eu^{3+} phosphors increased with an increase in the calcination temperature. The increase in luminescence intensity

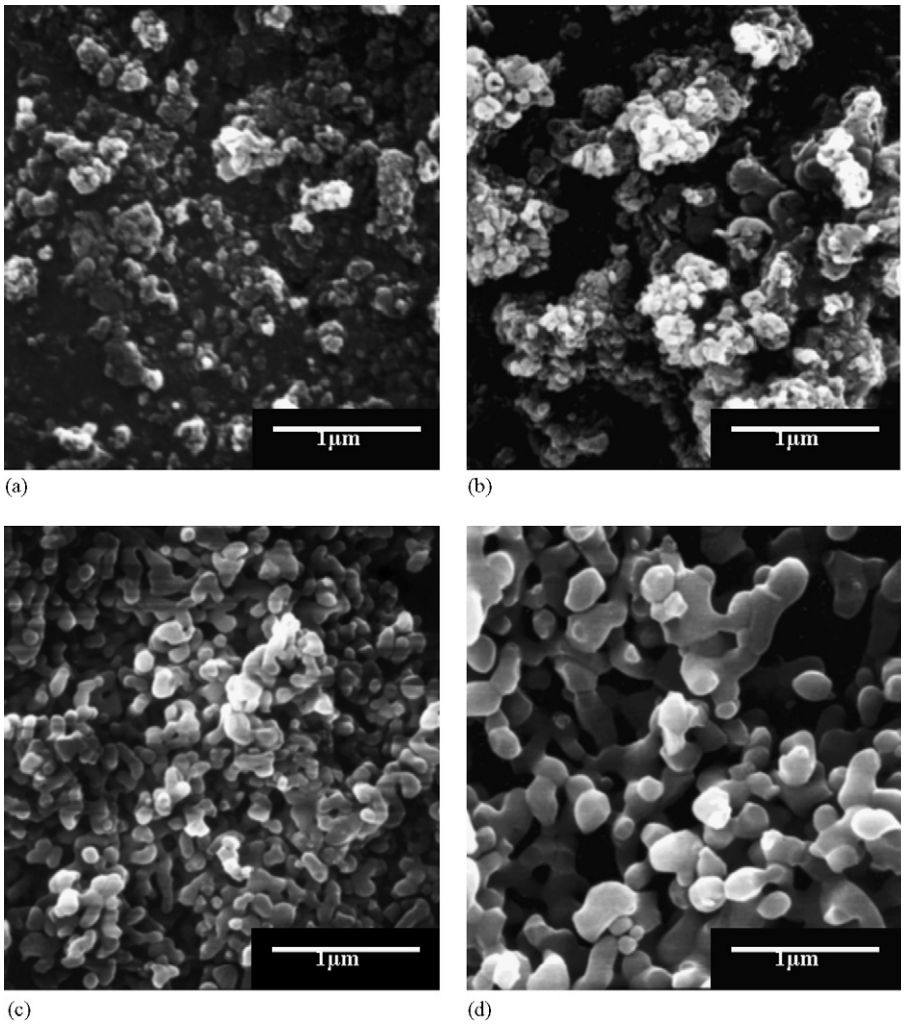

Fig. 2. Scanning electron micrographs of the sol–gel derived $(Y_{2.85}Eu_{0.15})Al_5O_{12}$ phosphors calcined for 2 h at (a) 900 °C, (b) 1000 °C, (c) 1200 °C, and (d) 1400 °C.

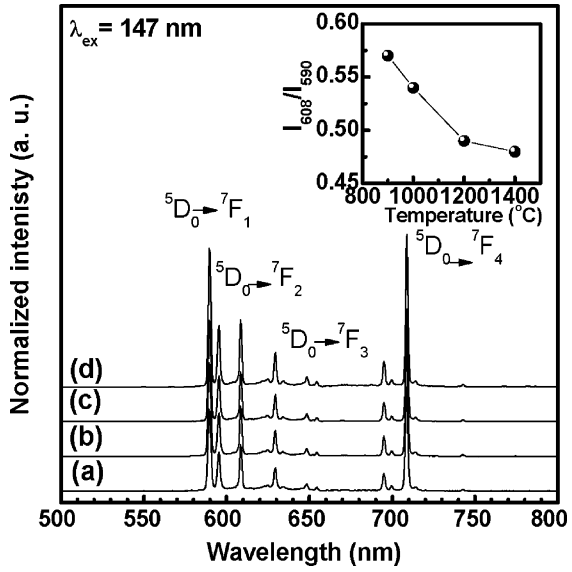

Fig. 3. Emission spectra ($\lambda_{excitation} = 147$ nm) of the sol–gel derived $(Y_{2.85}Eu_{0.15})Al_5O_{12}$ phosphors calcined for 2 h at (a) 900 °C, (b) 1000 °C, (c) 1200 °C, and (d) 1400 °C. Inset shows the dependence of the intensity ratio between emissions at 608 and 590 nm (I_{608}/I_{590}) on calcination temperature.

is due to improved phosphor crystallinity after calcination at elevated temperatures.

The emission spectra display a number of emission peaks in the wavelength range of 580–720 nm with prominent peaks at 590, 596, 608 and 709 nm. The emission spectra obtained for the sol–gel derived YAG:Eu^{3+} phosphors are similar in nature to those reported for YAG:Eu^{3+} prepared by solid-state reactions [1,2]. The assignment of the various emission peaks to transitions involving $^5D_0$ to the stark split sublevels of ^7F_J ($J = 1, 2, 3$ and 4) are also shown in Fig. 3. Two strong emission peaks at 590 and 709 nm were observed for all samples. On the other hand, the emission at 608 nm was consistently relatively weak. The emission peak at 590 nm corresponds to magnetic dipole transition ($^5D_0 \rightarrow {}^7F_1$) and the intensity of this transition is independent of the site symmetry of Eu^{3+} ions [16]. Whereas the emission peak at 608 nm corresponds to the forced electric dipole transition ($^5D_0 \rightarrow {}^7F_2$) and its intensity is very sensitive to the site symmetry of Eu^{3+} ions. A strong emission due to the hypersensitive transition ($^5D_0 \rightarrow {}^7F_2$) will appear when Eu^{3+} ions occupy a site without inversion symmetry. On the other hand, the absence of emission produced by hypersensitive transition ($^5D_0 \rightarrow {}^7F_2$) signifies the presence of inversion symmetry for Eu^{3+} ions [16].

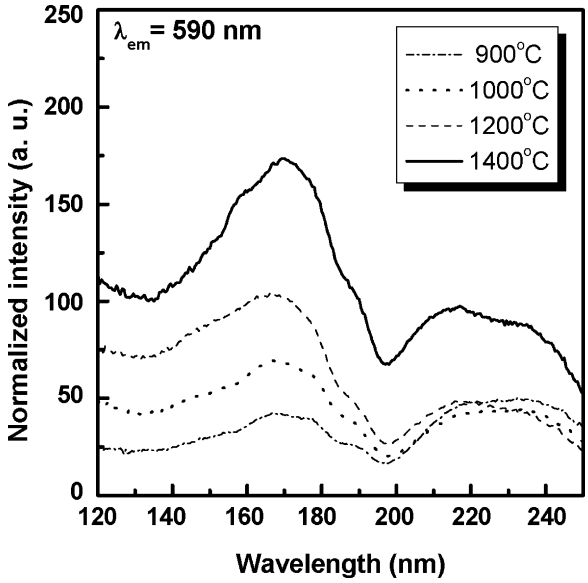

Fig. 4. Excitation spectra ($\lambda_{emission} = 590$ nm) of the sol–gel derived $(Y_{2.85}Eu_{0.15})Al_5O_{12}$ phosphors calcined for 2 h at 900, 1000, 1200, and 1400 °C.

The intensity ratio (I_{608}/I_{590}) between $^5D_0 \rightarrow {}^7F_2$ (at 608 nm) and $^5D_0 \rightarrow {}^7F_1$ (at 590 nm) transitions can be used to evaluate the site symmetry for Eu^{3+} [17,18]. The ratios calculated for the sol–gel derived samples are given in the inset of Fig. 3, which shows decreasing I_{608}/I_{590} ratio with an increase in the calcination temperature. This reveals that greater deviation from inversion symmetry is formed with lower calcination temperature. Since a decrease in the calcination temperature results in the formation of nanosized particles as illustrated in Fig. 2, it is reasonable to figure that the trend of increasing asymmetry at low temperatures is probably ascribed to the distorted chemical surroundings of the nano-sized particles.

Fig. 4 shows the excitation spectra of YAG:Eu^{3+} (5%) phosphors (system II) monitored at 590 nm emission using synchrotron radiation. The excitation spectra can be divided into two parts according to the band-gap energy level of YAG at 190 nm [19]. The excitation band at 178 nm corresponds to the fundamental absorption of YAG host [11], and the one at 238 nm is ascribed to the charge transfer between Eu^{3+}–O^{2-} pairs [10]. The excitation intensity of the 178 nm peak reduces with a decrease in the calcination temperatures. For the samples calcined at 900, 1000 and 1200 °C, the intensity of the excitation peak at 238 nm (the charge transfer band) is observed to be unchanged. Notably, the intensity of the excitation peak at 238 nm significantly increases for the sample calcined at 1400 °C. When the sol–gel derived precursors are calcined at low temperatures, nano-particles are formed with lots of surface defects due to their large surface-to-volume ratio. These defects provide an additional non-radiative relaxation path, thereby reducing the intensity. When the precursors are heated at elevated temperatures, enhanced excitation intensity is observed as a result of the larger particle size and fewer surface defects in the formed powder. Therefore, heating at elevated temperatures leads to increased luminescence, as shown in Fig. 4.

YAG:Eu^{3+} (5%) phosphors have been also prepared via the solid state reaction method. The powders were calcined at 1500 °C for 2 h. The quantum efficiencies of the phosphors prepared by the solid-state method and sol–gel method were measured and the values were about 8%. The obtained results consisted with the value reported by Dong and Deng [20]. The lifetimes of the phosphors were also measured. The lifetimes of the phosphors prepared by the solid-state process and the sol–gel process were 2.74 and 3.54 ms, respectively. The slight increase in lifetime for the sol–gel derived powders probably results from fewer defects formed in obtained powders because of the homogeneous compositional distribution and low calcination temperature in the sol–gel process.

3.2. Analysis of the crystal structure of non-stoichiometric YAG:Eu^{3+}

YAG exhibits a garnet structure. The unit cell of a garnet compound contains eight formula units with a general formula $A_3B_2C_3O_{12}$, where A stands for an ion A at dodecahedral sites, B denotes to an ion B located at octahedral site, and C represents to an ion C at tetrahedral site. According to the Wyckoff notation, these different symmetry sites can also be represented as 24(c), 16(a), and 24(d), respectively. The oxygen ions occupy in general positions, 96(h) in Wyckoff notation [21]. Each oxygen ion is a member of two dodecahedra, one octahedral, and one tetrahedron. In yttrium aluminum garnet, yttrium ions occupy the A site, and aluminum ions locate at the B and C sites [22]. Therefore, aluminum ions have two un-equivalent positions.

The effects of non-stoichiometry on the phase purity and crystal structure of the sol–gel derived YAG:Eu^{3+} phosphors are investigated. System II corresponds to the stoichiometric YAG:Eu^{3+} phosphors, and systems I and III represent, respectively, the phosphors containing deficient and excess aluminum ions. The sol–gel derived precursors in each system were calcined at 1400 °C for 2 h, and the resultant XRD patterns are illustrated in Fig. 5. In systems II and III, only the phase belonging to YAG is detected. On the other hand, trace amounts of $Y_4Al_2O_9$ (YAM) and $YAlO_3$ (YAP) are found in the aluminum-ion deficient sample (system I).

The Rietveld refinement method was adopted to analyze the effects of non-stoichiometry on the crystal structures of the prepared samples in three systems. The structural parameters of YAG, YAM and YAP are based on the values reported by Euler and Bruce [23], Yamane and Shimada [24] and Vastlechko et al. [25], respectively. The obtained reliability factor R_p is 11.87, 11.70 and 10.05% for systems I, II and III, respectively. This indicates that the content of YAG, YAM and YAP phases in system I is 0.9291 (3), 0.0551 (3) and 0.0158 (3) (in mol%), respectively. In the other two systems, only YAG was found. The simulated diffraction patterns of the samples in these three systems are illustrated in Fig. 6, where "+" marks represent the experimental diffraction data, the solid curves denote the simulated diffraction data, and the dotted lines indicate the deviation of the experimental values from the simulated values. Based on the reliability factors and the deviation curves illustrated, the refinement results provide consistent models of the crystal

Table 1
Occupancy of various sites in the sol–gel derived YAG:Eu^{3+} phosphors

	Occupancy						
	Oxygen-ion site	Yttrium-ion site	Eu^{3+} in yttrium-ion site	Aluminum-ion site (octahedral)	Eu^{3+} in aluminum-ion site (octahedral)	Aluminum-ion site (tetrahedral)	Eu^{3+} in aluminum-ion site (tetrahedral)
System I (m = 4.5)	1.0	0.96 (4)	0.04 (4)	0.99 (2)	0.01 (2)	1.0	0.0
System II (m = 5.0)	1.0	0.96 (4)	0.04 (4)	1.0	0.0	1.0	0.0
System III (m = 5.5)	1.0	0.93 (2)	0.04 (2)	1.0	0.0	1.0	0.0

The molar ratio of Y^{3+}, Al^{3+} and Eu^{3+} ions in each system is set to be 2.85:m:0.15, where m = 4.5, 5 and 5.5 for system I, II and III, respectively.

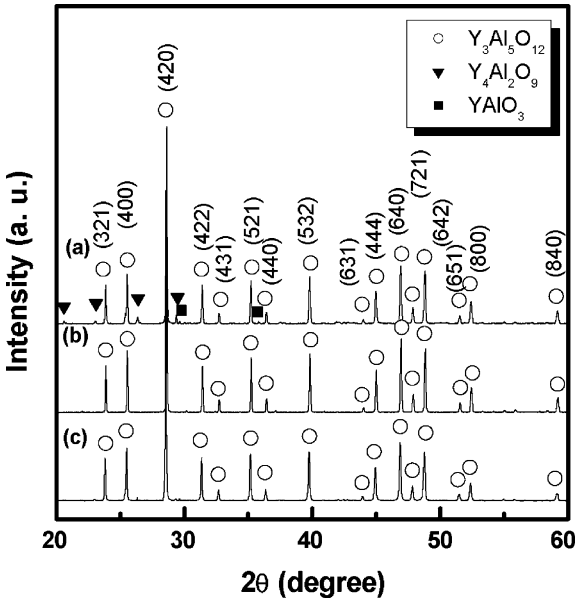

Fig. 5. X-ray diffraction patterns of the sol–gel derived YAG:Eu^{3+} phosphors calcined at 1400 °C for 2 h: (a) $1.425Y_2O_3$–$0.075Eu_2O_3$–$2.25Al_2O_3$ (system I), (b) $1.425Y_2O_3$–$0.075Eu_2O_3$–$2.5Al_2O_3$ (system II), and (c) $1.425Y_2O_3$–$0.075Eu_2O_3$–$2.75Al_2O_3$ (system III).

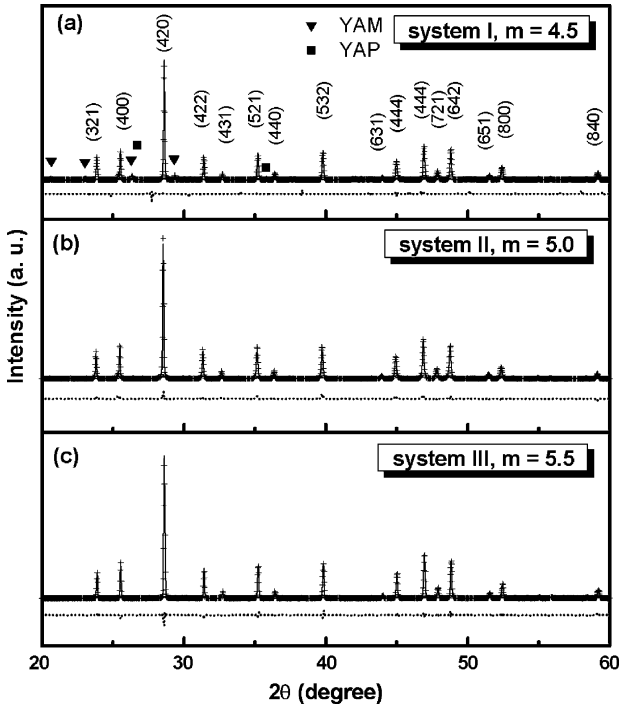

Fig. 6. Rietveld refinement results of the sol–gel derived phosphors calcined at 1400 °C for 2 h: (a) $1.425Y_2O_3$–$0.075Eu_2O_3$–$2.25Al_2O_3$ (system I), (b) $1.425Y_2O_3$–$0.075Eu_2O_3$–$2.5Al_2O_3$ (system II), and (c) $1.425Y_2O_3$–$0.075Eu_2O_3$–$2.75Al_2O_3$ (system III).

structure of the samples in each system. The Rietveld refinement results of the samples in these three systems are summarized in Tables 1 and 2.

Table 1 lists the occupancy of the sites in YAG phase in each system. For the stoichiometric sample (system II), all Eu^{3+} ions enter into yttrium-ion sites of the YAG phase. For system III, the occupancy of Eu^{3+} ions was found at around 4% in the yttrium-ion sites and 0% in the aluminum-ion sites. However, the overall occupancy of all cations in yttrium sites is noted to be much less than unity in system III suggesting that certain vacancies are introduced into the yttrium-ion sites due to the presence of excess aluminum ions. In system I, the occupancy of Eu^{3+} in the yttrium-ion sites is similar to that in the other two systems. However, 1% of Eu^{3+} ions are observed to enter into the octahedral sites of aluminum ions revealing the entrance of Eu^{3+} ions into both aluminum-ion and yttrium-ion sites in system I. In

Table 2
Lattice parameters of the sol–gel derived YAG:Eu^{3+} phosphors

		Lattice constant					
		a	b	c	α	β	γ
System I (m = 4.5)	YAG	12.0391 (4)	12.0391 (4)	12.0391 (4)	90.000	90.000	90.000
	YAM	7.4063 (3)	10.4732 (1)	11.1043 (2)	90.000	108.680 (5)	90.000
	YAP	5.3306 (5)	7.3765 (6)	5.1795 (4)	90.000	90.000	90.000
System II (m = 5.0)	YAG	12.0267 (5)	12.0267 (5)	12.0267 (5)	90.000	90.000	90.000
System III (m = 5.5)	YAG	12.0066 (3)	12.0066 (3)	12.0066 (3)	90.000	90.000	90.000

YAG, YAM, and YAP refer to the phases of $Y_3Al_5O_{12}$, $Y_4Al_2O_9$, and $YAlO_3$, respectively.

addition, no vacancies were observed at aluminum-ion sites in system I. This phenomenon is considered attributable to the formation of the yttrium-rich impurity phases (YAP and YAM) that effectively consume excess yttrium ions. The Rietveld analysis also confirmed that no Eu^{3+} ions enter into either aluminum-ion sites or yttrium-ion sites in the YAP and YAM phases.

The calculated lattice parameters of the samples in the three systems are summarized in Table 2. It reveals that the lattice constant of $(Y_{2.85}Eu_{0.15})Al_5O_{12}$ (system II) is 12.0267 (5) Å, which is slightly larger than that of $Y_3Al_5O_{12}$ (12.000 Å) [19] because Y^{3+} ions are substituted by Eu^{3+} ions having a larger radius. The calculated Al–O band lengths in the octahedral and tetrahedral sites are 1.922 (4) and 1.782 (4) Å, respectively, which are similar to those reported for $Y_3Al_5O_{12}$ [19]. However, the Y–O bond lengths in the dodecahedral sites are 2.316 (5) and 2.433 (5) Å, which are slightly larger than the reported values [19]. The slight increase in the bond-length is associated with the substitution by Eu^{3+} ions at Y^{3+} site.

On the other hand, the aluminum-ion deficient system (system I) is much more complicated than system II due to the co-existence of the impurity phases $Y_4Al_2O_9$ (YAM) and $YAlO_3$ (YAP). The adjusted lattice parameter of YAG in system I is 12.0391 (4) Å, which is larger than that in system II. In system I, europium ions occupy both the yttrium-ion and aluminum-ion sites (Table 1). Since the ionic size of Eu^{3+} (0.95 Å) is much larger than that of Al^{3+} (0.54 Å), the large lattice parameters in system I can be attributed to the partial substitution by Eu^{3+} ions at the aluminum-ion sites in system I. The lattice parameters of YAM [23] and YAP [25] are listed in Table 2, which are similar to those reported in the previous studies. The lattice parameters and bond lengths for system III are also listed in Table 2. These values are close to those reported for pure $Y_3Al_5O_{12}$ [19], indicating less degree of structural distortion occurring in system III.

3.3. Luminescence characteristics of non-stoichiometric YAG:Eu^{3+} phosphors

Fig. 7 depicts the emission spectra of the 1400 °C-calcined samples in these three systems upon 147 nm excitation using synchrotron radiation. The emission peaks in the three samples, regardless of the *m* value, correspond to the characteristic emission of Eu^{3+} ions in the host of YAG. In system I, the emission of europium-ion doped yttrium aluminum monoclinic (YAM:Eu^{3+}) and europium-ion doped yttrium aluminum perovskite (YAP:Eu^{3+}) is not observed in the emission spectra as shown in Fig. 7(a), implying that Eu^{3+}-ion substitution occurs in YAG lattice rather than in YAM and YAP lattices. This observation is consistent with the Rietveld refinement results described in the previous section.

It is noted that the emission intensity at 590 nm of the prepared phosphors increases with the value of *m*. The presence of the impurity phases (YAM and YAP) in system I probably provide a non-radiative path and thereby reduce the luminescence. As mentioned earlier, the intensity ratio (I_{608}/I_{590}) between $^5D_0 \rightarrow {}^7F_2$ (at 608 nm) and $^5D_0 \rightarrow {}^7F_1$ (at 590 nm) transitions can be used to assess the deviation from inversion symmetry. The

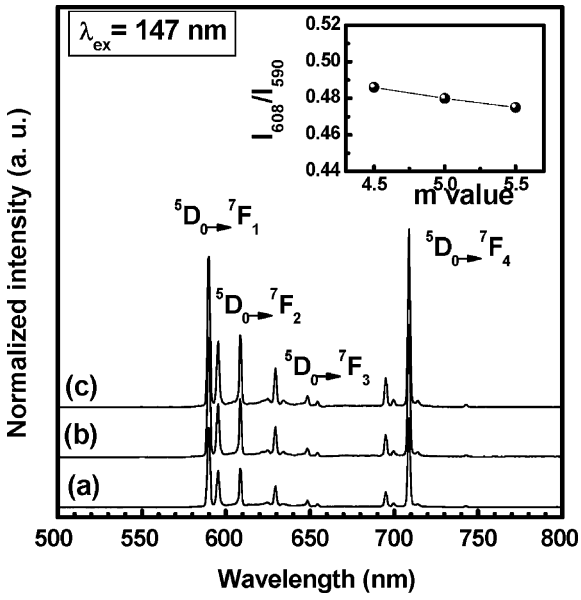

Fig. 7. Emission spectra ($\lambda_{excitation} = 147$ nm) of the sol–gel derived phosphors: (a) $1.425Y_2O_3$–$0.075Eu_2O_3$–$2.25Al_2O_3$ (system I), (b) $1.425Y_2O_3$–$0.075Eu_2O_3$–$2.5Al_2O_3$ (system II), and (c) $1.425Y_2O_3$–$0.075Eu_2O_3$–$2.75Al_2O_3$ (system III). Inset shows the dependence of the intensity ratio (I_{608}/I_{590}) on the value of *m*.

changes in the I_{608}/I_{590} ratio with various *m* values are illustrated in the inset of Fig. 7. A slight decrease in the I_{608}/I_{590} ratio is observed with increasing m value, suggesting that the anionic environment around Eu^{3+} ions the aluminum-ion excess sample (system III) is more symmetrical than that in systems I and II. The morphological investigations also indicate less structural distortion in system III. There is no inconsistency between the structural analysis and luminescence properties results for system III.

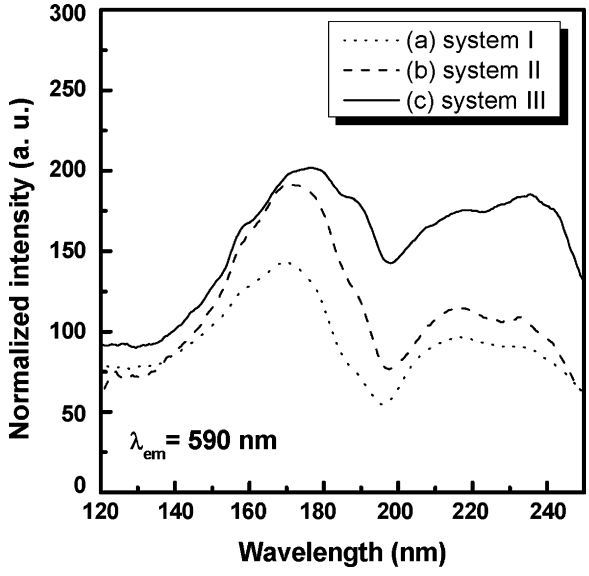

Fig. 8. Excitation spectra ($\lambda_{emission} = 590$ nm) of the sol–gel derived phosphors: (a) $1.425Y_2O_3$–$0.075Eu_2O_3$–$2.25Al_2O_3$ (system I), (b) $1.425Y_2O_3$–$0.075Eu_2O_3$–$2.5Al_2O_3$ (system II), and (c) $1.425Y_2O_3$–$0.075Eu_2O_3$–$2.75Al_2O_3$ (system III).

The VUV excitation spectra of YAG:Eu^{3+} phosphors recorded at 590 nm emission for systems I–III are illustrated in Fig. 8. The excitation spectra reveal a charge transfer band at 238 nm and an excitation band at 178 nm that is lower than the wavelength of the host absorption (190 nm). The intensities of the charge transfer band and host absorption band both increase with the aluminum ion content, indicating that varying the amount of aluminum ions in YAG:Eu^{3+} phosphors affects the crystal structure as well as the emission and excitation intensities. A shoulder at 185 nm is observed in system III. Since yttrium vacancies were found in the aluminum-ion excess YAG:Eu^{3+} sample based on the Rietveld refinement results, the excitation band at 185 nm in system III is possibly related to the excitons associated with yttrium vacancies. The VUV luminescence investigations reveal that the sol–gel derived YAG:Eu^{3+} phosphors with reduced particle sizes and improved luminescence characteristics possess great potential for application to plasma display panels.

4. Conclusions

Nano-sized YAG:Eu^{3+} phosphors were successfully prepared via the sol–gel route employing citric acid and ethylene glycol as the polymerizing agents. VUV-excited luminescence studies indicate that two major excitation peaks formed at 178 and 238 nm were responsible for generating the characteristic red emission of Eu^{3+} ions. Increasing the calcination temperature results in a more symmetric anionic environment for Eu^{3+} ions in the host of YAG and enhanced emission intensity. The Rietveld refinement analysis reveals that the aluminum ion content significantly affects the crystal structure and the occupancy in different cationic sites. Increasing the aluminum-ion content results in enhanced luminescence intensity and a less distorted anionic environment for the Eu^{3+} ions. A reduced particle size and improved emission characteristics were obtained for the sol–gel derived YAG:Eu^{3+} phosphors via controlling the synthesis conditions and chemical compositions.

Acknowledgements

The authors would like to thank Mr. Hong-Kai Cheng at National Synchrotron Radiation Research Center (NSRRC), Taiwan for his help in measuring the VUV excitation spectra. The authors would like to thank Dr. Jyh-Fu Lee and Dr. Hwo-Shuenn Hsu at NSRRC for their assistance in analyzing the crystal structure. The authors would also like to thank National Science Council of the Republic of China, Taiwan for financially supporting this research under contract no. NSC 94-2214-E002-005.

References

[1] J.A. Koningstein, Phys. Rev. 136A (1964) 717.
[2] M. Sekita, H. Haneda, S. Shirasaki, T. Yanagitani, J. Appl. Phys. 69 (1991) 3709.
[3] I. Matsubara, M. Parathaman, S.W. Allison, M.R. Cates, D.L. Beshears, D.E. Holcomb, Mater. Res. Bull. 35 (2000) 217.
[4] G.Y. Hong, B.S. Jeon, Y.K. Yoo, J.S. Yoo, J. Electrochem. Soc. 148 (2001) H161.
[5] Y.H. Zhou, J. Lin, S.B. Wang, H.J. Zhang, Opt. Mater. 20 (2002) 13.
[6] Y.H. Zhou, J. Lin, S.M. Han, S.B. Wang, H.J. Zhang, Mater. Res. Bull. 38 (2003) 1289.
[7] Y. Zhou, J. Lin, M. Yu, S. Wang, J. Alloys Compd. 375 (2004) 93.
[8] C.H. Lu, W.T. Hsu, J. Dhanaraj, R. Jagannathan, J. Eur. Ceram. Soc. 24 (2004) 3723.
[9] G. Xia, S. Zhou, J. Zhang, S. Wang, Y. Liu, J. Xu, J. Crystal. Growth 283 (2005) 257.
[10] Y.P. Fu, J. Alloys Compd. 402 (2005) 233.
[11] A. Mayolet, W. Zhang, E. Simoni, J.C. Krupa, P. Martin, Opt. Mater. 4 (1995) 757.
[12] H.M. Rietveld, J. Appl. Crystallogr. 2 (1969) 65.
[13] X. Guo, K. Sakurai, Jpn. J. Appl. Phys. 39 (2000) 1230.
[14] I. Matsubara, M. Paranthaman, S.W. Allison, M.R. Cates, D.L. Beshears, D.E. Holcomb, Mater. Res. Bull. 35 (2000) 217.
[15] B.D. Cullity, S.R. Stock, Elements of X-ray Diffraction, Prentice Hall, NJ, 2001, p. 170.
[16] G. Blasse, B.C. Grabmier, Lumin. Mater., Springer-Verlag, 1994, p. 44.
[17] W.C. Nieupoort, G. Blasse, Proceedings of the John Hopkins University Conference, Inter Science, NY, 1967, p. 161.
[18] T. Ishizaka, Y. Kurokawa, J. Appl. Phys. 90 (2001) 243.
[19] C.W. Thiel, H. Cruguel, Y. Sun, G.J. Lapeyre, R.M. Macfarlane, R.W. Equall, R.L. Cone, J. Lumin. 94–95 (2001) 1.
[20] J. Dong, P. Deng, J. Lumin. 104 (2003) 151.
[21] D.A. Pawlak, K. Wozniak, Z. Frukacz, T.L. Barr, D. Fiorentino, S. Seal, J. Phys. Chem. B 103 (1999) 1454.
[22] Y.N. Xu, W.Y. Ching, Phys. Rev. B 59 (16) (1999) 10530.
[23] F. Euler, J.A. Bruce, Acta Crystallogr. 19 (1965) 971.
[24] H. Yamane, M. Shimada, J. Solid State Chem. 141 (1998) 466.
[25] L. Vastlechko, A. Matkovskii, D. Savytskii, A. Suchocki, F. Wallrafen, J. Alloys Compd. 291 (1999) 57.